

We are IntechOpen, the world's leading publisher of Open Access books Built by scientists, for scientists

6,900

Open access books available

186,000

International authors and editors

200M

Downloads

Our authors are among the

154

Countries delivered to

TOP 1%

most cited scientists

12.2%

Contributors from top 500 universities



WEB OF SCIENCE™

Selection of our books indexed in the Book Citation Index
in Web of Science™ Core Collection (BKCI)

Interested in publishing with us?
Contact book.department@intechopen.com

Numbers displayed above are based on latest data collected.
For more information visit www.intechopen.com



Electrical Breakdown Behaviors in Microgaps

Guodong Meng and Yonghong Cheng

Abstract

The study of electrical breakdown behaviors in microgaps has drawn intensive attention around the world due to the miniaturization of electronic devices that allows electronic circuits to be packaged more densely, making possible compact computers, advanced radar and navigation systems, and other devices that use very large numbers of components. Therefore, a clear understanding of the electrical breakdown behaviors in microgaps is required to avoid the dielectric breakdown or to trigger the breakdown at microscale. This chapter introduces the significance of understanding breakdown characterization and reliability assessment for electrostatically actuated devices, magnetic recording devices, photomasks, RF MEMS switches, and micromachines and points out the derivation of the classical Paschen's law at microscale. Then it summarizes the state-of-the-art research work on the methodology, influencing factors, dynamics, and physical mechanisms of electrical breakdown in microgaps, which is expected to expand the general knowledge of electrical breakdown to the microscale regime or more and benefits the reliability assessment and ESD protection of microscale and nanoscale devices.

Keywords: electrical breakdown behaviors, microscale, Townsend avalanche, field emission, influencing factors, dynamics, physical mechanism

1. Introduction

1.1 Background and motivation

Device miniaturization has revolutionized electronics, allowing denser packaging of electronic circuits to make possible compact computers, advanced radar and navigation systems, and other devices that use very large numbers of components [1]. In practical applications, micro-electromechanical systems (MEMSs), like micromachines and micro-mirror arrays, function by electrostatic actuation [2, 3], while the electronic devices, like photomasks [4, 5] and magnetoresistive (MR), giant magnetoresistive (GMR), and tunneling magnetoresistive (TMR) devices used in the magnetic recording industry [6–8], are at risk of accumulating static charges and the consequent threats of electrostatic discharge (ESD); both the microdevices and microstructures are associated with a strong electric field strength within microgaps [9]. For instance, the high operating voltages required for RF MEMS switches [10–13], micro-motors [14, 15] and micro-mirror [16, 17] can create sparking or breakdown across microgap structures due to electrical overstress (EOS) that may damage or destroy sensitive equipment, especially when the devices are subjected to a complex electromagnetic environment [7, 18].

Besides, the photomasks, which are used in front-end semiconductor photolithography processing to project a desired pattern onto the wafer surface, could become charged and a spark can occur either due to the real charge on the chrome guard ring or the induced charge caused by fields from surface charge on the quartz [4, 19]. Meanwhile, multiple applications in combustion, chemistry, biology, and medicine require the intentional creation of microplasmas or microdischarges [20, 21]. For instance, various microelectric propulsion systems have been proposed for ultra-small satellites, including Hall thrusters or pulsed plasma thrusters [22–25], which utilize microdischarges. As the devices are getting smaller from microscale to nanoscale and even molecular scale, the reliability assessment and underlying physics about the static charge and ESD events draw increasing attentions from both academics and industry [26–28]. Hence, predicting dielectric breakdown thresholds and figuring out the physical mechanism of microgap structures are critical to avoid undesired discharge or improve the microplasma performance, which would be of great interest to the microelectronic and plasma communities.

1.2 Derivation from the classical Paschen's law

The gas breakdown phenomenon was recognized ever since the creation of human beings thousands of years ago, but firstly systematically investigated by German physicist Paschen in 1889 [29]. Through conducting a series of electrical discharge experiments, Paschen established the widely used Paschen's law, which described the relationship between the breakdown voltage V_{bd} and the product of the pressure p and gap length d . Since then, Paschen's law has been employed for predicting breakdown thresholds and insulation performance of power equipment, electronic devices, etc.

Generally, Paschen's law could be explained by the Townsend avalanche mechanism, which considers that the electrons collide and ionize with neutral particles (α process) and positive ions bombard the cathode and generate secondary electrons (γ process), which are the primary processes during the discharge. Paschen's law could be described by the equation

$$U_{bd} = \frac{Bpd}{\ln(Apd) - \ln(\ln(1 + 1/\gamma))} \quad (1)$$

where U_{bd} is the breakdown voltage, d is the gap separation, p is the gas pressure, γ is the secondary electron emission coefficient, and A and B are constants determined by the gap type.

While the classical Paschen curve has a right branch with the breakdown voltage decreasing as pd decreases, a characteristic minimum, and a left branch with the breakdown voltage increasing as pd decreases, research has shown that the left branch continues to decrease nearly linearly with d , that is, in microscale gaps, pd scaling fails. Early experiments noted that reducing gap sizes to microscale at atmospheric pressure led to deviations in the traditional breakdown mechanism driven by Townsend avalanche and represented mathematically by Paschen's law (PL) [30]. Departing from the traditional PL, the breakdown voltage would undergo a plateau when the gap width is smaller than $\sim 10 \mu\text{m}$ and then continue to decrease with the gap width. The gap widths for the transition processes vary with the experimental conditions, such as electrode materials, electrode geometry, applied voltage waveform, gap pressures, etc.

Since the derivation of Paschen's law in the microscale regime was discovered in 1950s, a large number of research work has been dedicated to modification of the classical Paschen's law, from experimental investigation [31, 32] to numerical

simulation [33, 34], from atmosphere environment [35] to vacuum [36, 37]. Torres et al. and Slade et al. carried out a series of experimental investigations on microgap breakdown in air and vacuum, respectively. They both found out the plateau stage in the modified Paschen's law and the transition point of gap widths was 4 μm . Besides the numerical simulation, analytic and theoretical calculations have been also carried out. Go [38], Klas [39, 40], Buendia [41], and Loveless [42] calculated the breakdown thresholds at microscale coupling with field emission and Townsend avalanche, considering the ion-enhance field emission, where the electron collision ionization coefficient α and the secondary electron emission coefficient γ dictate the breakdown process, where the secondary electron emission coefficient γ would be enhanced by the space charge accumulation and the cathode charge production through secondary emission. Therefore, the investigation of electrical breakdown behaviors at microscale, including the methodology, fundamental properties, influencing factors, and physical mechanisms, is urgently demanded, which is of critical importance not only for the plasma physics community but also for micro-/nanoelectronic industries.

1.3 The main chapter content

This chapter summarizes the state-of-the-art methodologies, influencing factors, dynamics, and physical mechanisms of the electrical breakdown in microscale based on the research work in the last two decades.

Section 2 summarizes the methodology for investigating the electrical breakdown in microgaps. Section 3 summarizes the influencing factors of the electrical breakdown in microgaps. Section 4 and 5 summarize the dynamic process and physical mechanism of the electrical breakdown in microgaps. Summary and outlook are provided in Section 6.

2. Methodology

Different from the routine gas breakdown experiments in large gaps ($>0.1\text{ mm}$), the electrical breakdown experiments in microgaps ($<0.1\text{ mm}$) require a much better spatial resolution in terms of both observation and gap adjustment. Accordingly, the methodology is very diverse, including the macro electrode structure prepared by the mechanical technique, the planar electrode structure and MEMS device structure prepared by the microfabrication technique, and the microelectrode structure prepared by the electrochemical etching technique. Moreover, the in-situ electro-optical measurement technique has also been proposed for exploring the breakdown dynamic process at microscale. In this chapter, various experimental methods are discussed and summarized.

2.1 The macroelectrode structure

At the initial stage, the study was basically conducted with the macroelectrode structure and experimental setup similar to that at macroscale. **Figure 1a** shows the schematic diagram of a typical macro electrode-based experimental setup and (b) shows the picture of a spherical electrode-based experimental setup used in the literature. The electrode size is in the order of millimeters in radius, which could be fabricated by mechanical machining. One electrode is fixed with the base (also known as static electrode) and the other is movable with the screw micrometer or stepping motor (also known as movable electrode). Both electrodes are required to be aligned on a straight line to ensure the consistence of the discharge experiments.

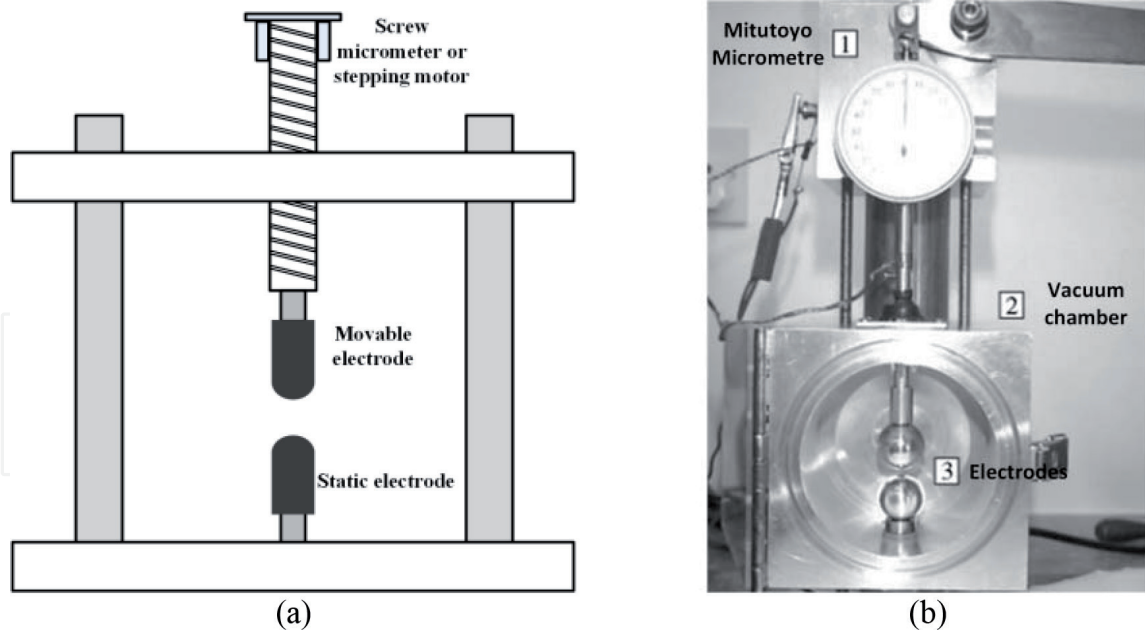


Figure 1.

(a) Schematic diagram of macroelectrode-based experimental setup. The gap distance is controlled and adjusted by the screw micrometer or stepping motor [43]; (b) the picture of two spherical electrode experimental setup for vacuum breakdown test [44].

Therefore, the gap distance could be controlled by adjusting the screw micrometer or stepping motor, with an accuracy of $2\ \mu\text{m}$. Therefore, this method applies for the electrical breakdown in microgaps ranging from 5 to $500\ \mu\text{m}$.

2.2 The planar electrode structure

The emerging of microelectronic devices drew intensive attention to the electrical reliability issues, and thus, the planar electrode structure was proposed. Through the standard fabrication process, such as oxidation, lithography, deposition, etching, etc., the planar metal electrode (aluminum, copper, gold, and platinum) is patterned on the silicon dioxide/silicon substrate with a thickness of several hundreds of nanometers and a gap distance ranging from several nanometers to micrometers.

(a) shows the typical planar electrode-based experimental setup. The semi-circular type electrode pattern was fabricated on the substrates and the electrical breakdown experiments could be conducted between microgaps. In addition, the suspended planar electrode was also proposed by sacrificing layer process as shown in **Figure 2b**, in which electrical breakdown properties of MEMS devices (such as MEMS switches and MEMS motors) could be investigated. Therefore, this method is dedicated to the study of device reliability issues with typical and simple structures.

2.3 The MEMS device structure

Apart from the typical simplified electrode structures above, lots of research work has also focused on the breakdown characterization and reliability assessment of real device structures under ESD impact, especially for those devices that require electrostatic actuation (i.e., RF MEMS switch, micro-motor, and micro-mirror) or are very susceptible to static charge accumulation (i.e., photomask). **Figure 3** shows the pictures of different RF MEMS devices for ESD impact testing, which are gold-based capacitive (a) and ohmic (b–d) RF-MEMS switches with vertical air-gap structure from 1.0 to $4.5\ \mu\text{m}$ and lateral air-gap structure of $6.7\ \mu\text{m}$. For this

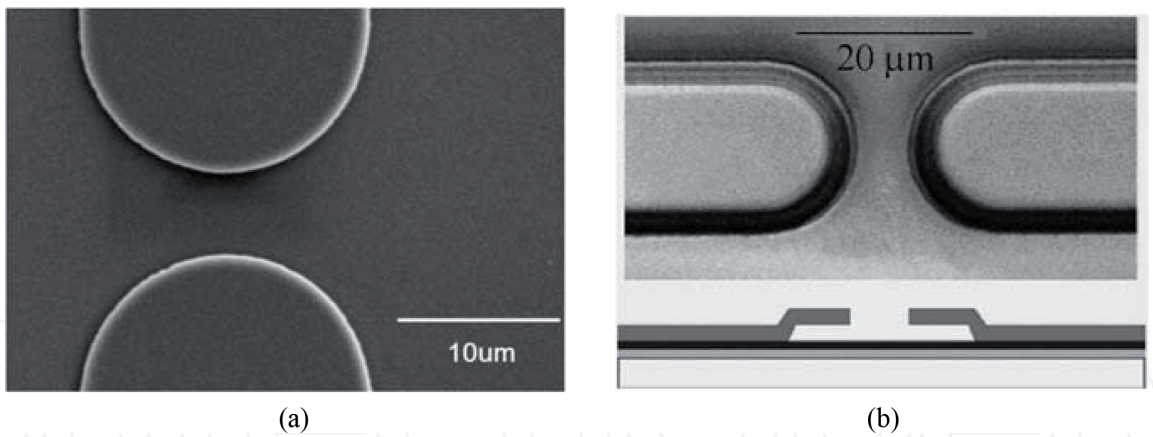


Figure 2. Schematic diagram of planar electrode-based experimental setup: (a) semicircular type electrode [45] and (b) suspended semicircular type electrode [46].

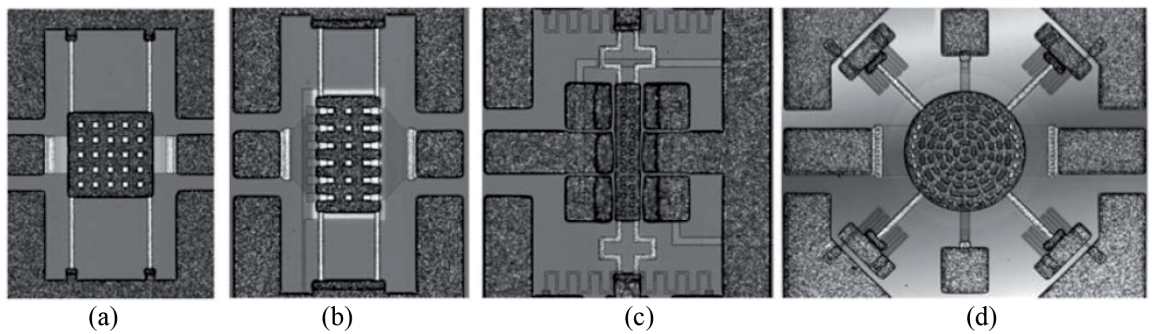


Figure 3. Tested devices were gold-based (a) capacitive and (b–d) ohmic RF-MEMS switches [10].

configuration, the breakdown may occur across the micron air gaps of RF MEMS switches and result in permanent physical damage on the devices.

Figure 4a shows the SEM image of a torsional ratcheting actuator (TRA) in which the ratchet gear and curved comb fingers are used for electrostatic actuation and (b) shows the optical image of metal-air-metal device on reticle with 4 μm gap,

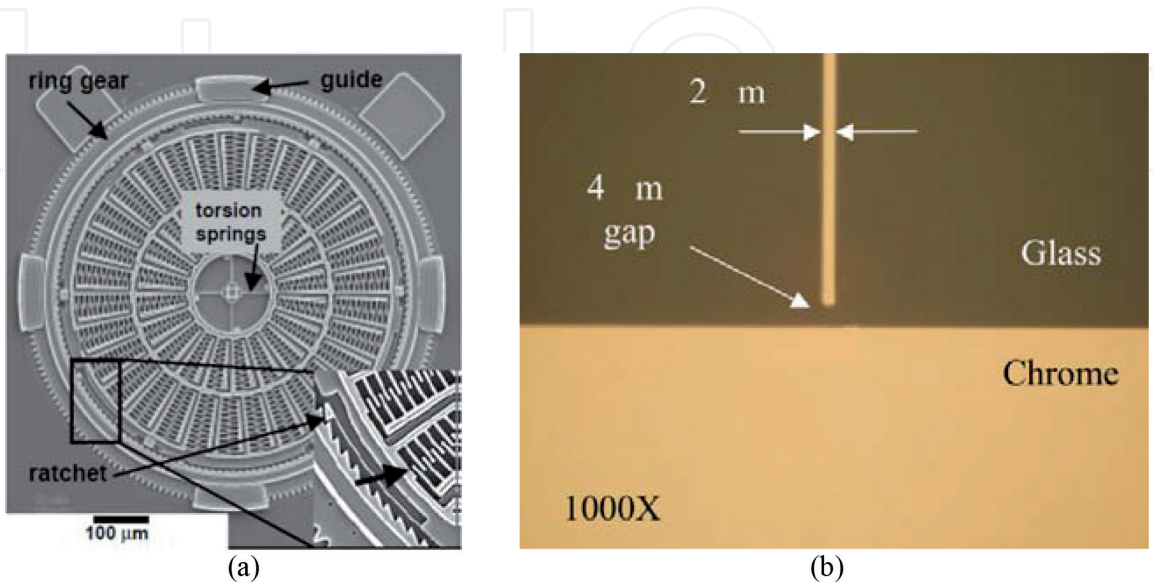


Figure 4. (a) SEM image of a torsional ratcheting actuator (TRA). The inset shows an enlarged view of the ratchet gear and curved comb fingers used for electrostatic actuation [15]; (b) optical image of metal-air-metal device on reticle with 4 μm gap [7].

which has been developed to check the ESD threat to reticles in a photolithography bay. For this configuration, the breakdown may occur across the surface of the air-gap structure and result in permanent physical damage on the devices.

2.4 The microelectrode structure

While the planar electrode and MEMS device structure are employed to explore the electrical reliability of microelectronic devices, the intrinsic properties of electrical breakdown in microgaps require microelectrodes with precisely controllable morphology and geometry, which were proposed and fabricated by combining the electrochemical etching and Joule melting method [47]. **Figure 5** shows the microelectrode structure-based experimental setup, of which the hemisphere electrodes were made of tungsten, and the radius of the electrodes ranged from 50 nm to 200 μm . The hemisphere electrodes have a regular and contaminant-free surface. The three-dimensional piezoelectric displacement could align the electrode pair with the aid of an optical microscope, allowing precise gap adjustment from 1 to 25 μm with an uncertainty of ± 100 nm.

2.5 The in-situ electro-optical experimental setup

Basically, the fundamental properties and influencing factors of the electrical breakdown in microgaps could be obtained by measuring the electrical parameters; however, to further understand the dynamics and physical mechanism, additional physical parameters during the breakdown are required. Monitoring the optical properties of the breakdown dynamic process is the primary way, which may need to satisfy two requirements simultaneously: (1) how to observe the breakdown channel at microscale and (2) how to capture the breakdown appearance in nanoseconds.

Figure 6 shows the electro-optical measurement setup that can simultaneously fulfill these requirements. The system consists of a nanosecond pulse generation unit, a synchronous and delay triggering unit, an in-situ optical imaging unit, and an electrical parameter measurement unit. The nanosecond pulse generation unit can provide amplitude-adjustable pulses up to 5 kV. The synchronous and delay triggering unit is achieved by a dual-channel function signal generator which can adjust the relative time delay between the two TTL triggering signals and ensure the synchronism of the test. The in-situ optical imaging unit integrates the optical microscope for micron-scale spatial resolution (1 μm) and the high-speed gated ICCD camera for nanosecond-scale temporal resolution (2 ns). The breakdown current and voltage are measured by a current coil (1 A/V) and a voltage attenuator (100:1), and then recorded by a digital oscilloscope. This system allows temporal

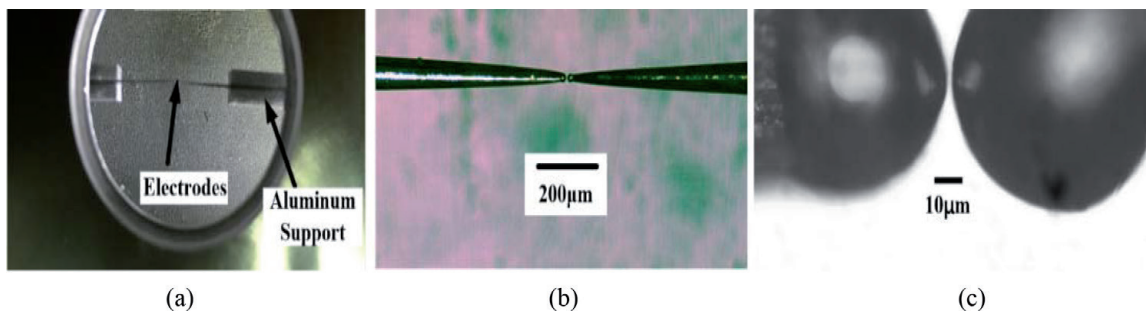


Figure 5. Schematic diagram of sphere-to-sphere microelectrode-based experimental setup: (a) 10 \times , (b) 50 \times , and (c) 1000 \times magnification [48].

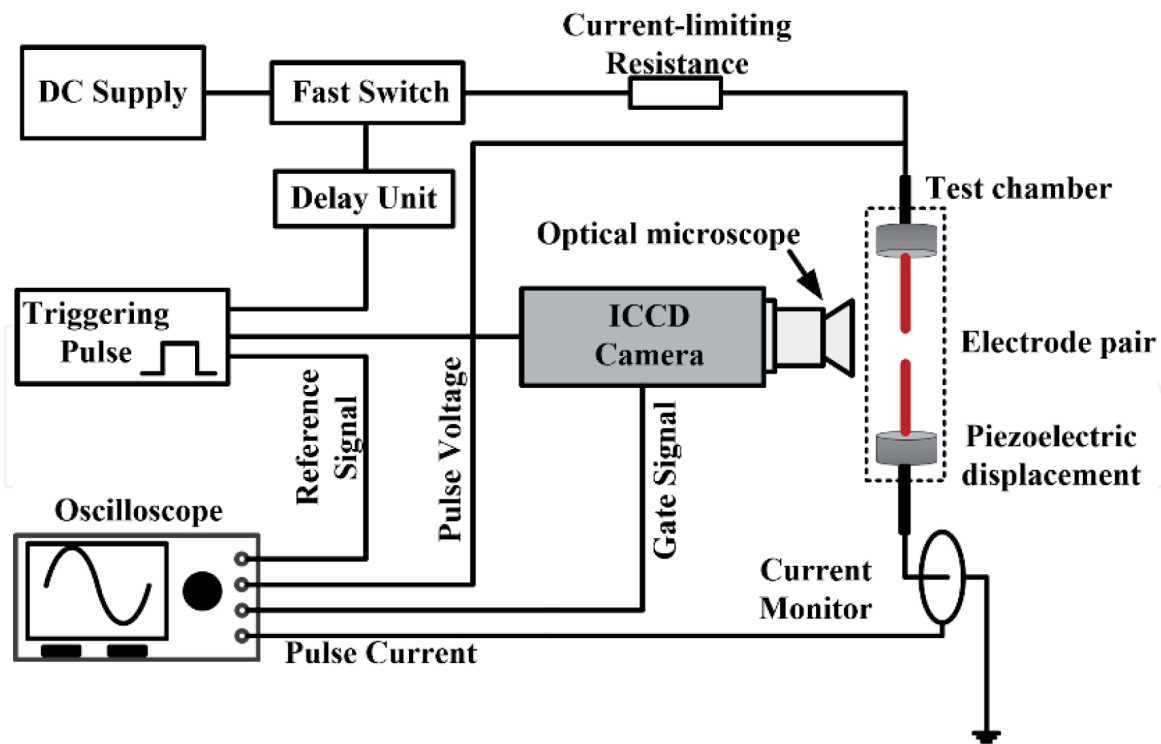


Figure 6.
 Schematic diagram of in-situ electro-optical measurement system [48, 49].

and spatial-resolved optical measurement and images the discharge appearance of pulse breakdown across microgaps, which will be a promising method to further explore the underlying principle of gas breakdown at microscale and evaluate the insulation performance in micro-/nanoelectronics.

3. Influencing factors of electrical breakdown in microgaps

As the gap size decreases, the classical Paschen's law demonstrates a significant derivation at microscale which implies the different physical mechanisms from Townsend avalanche breakdown. Since a lot of influencing factors could affect the electrical breakdown, this section gives some of the influencing factors such as the gap widths, the atmospheric pressures, and the applied voltages. These results determine quantitative relationships between the breakdown and the factors, and thus provide an overall picture of the electrical breakdown in microgaps.

3.1 The effect of the gap widths

Figure 7 shows the breakdown thresholds as a function of gap width in atmospheric air (101 kPa) at room temperature (298.15 K). The electrode configuration is hemisphere-hemisphere with gap widths from 1 to 25 μm . For gap widths $< 5 \mu\text{m}$, the breakdown voltage decreases with decreasing gap width. For gap widths between 5 and 10 μm , the breakdown voltages almost remain constant at about 490V regardless of the gap width, demonstrating a "plateau" stage. Although numerous microscale breakdown studies have noted this plateau [50], a strong hypothesis has not yet been developed. For gap widths larger than 10 μm , breakdown voltage increases dramatically with increasing gap width, indicating the increasing importance of Townsend avalanche. It can be noted that the breakdown voltage is 386 V when the gap width is 1 μm and the breakdown voltage is 842 V when the gap width is 25 μm . As the gap width shrinks to several micrometers, the

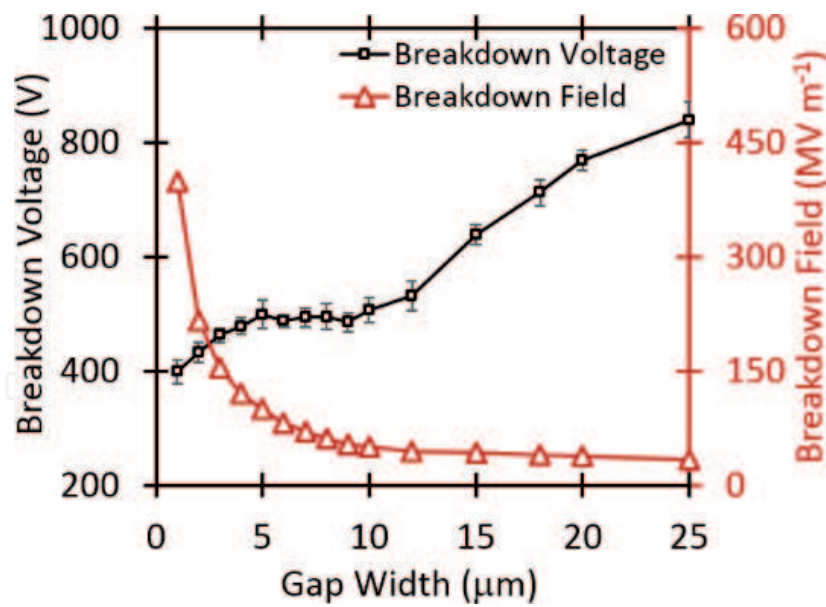


Figure 7. Measured breakdown voltage and electric field as a function of gap widths, the error bars represent the standard deviation of the measured breakdown voltage.

number of gas molecules inside the gap would be not enough for impact ionization, thus higher field strength is demanded for electron avalanche. When the gap width is reduced to $<5 \mu\text{m}$, the electric field strength is calculated to be $\sim 10^8 \text{ V/m}$, which has reached the threshold of field electron emission from the electrode surface. The obvious transition in the curves can be noticed and the cathode field emission plays a dominant role in the generation of free electrons.

3.2 The effect of applied voltages

Figure 8 shows the breakdown thresholds as a function of applied voltages in atmospheric air (760 Torr) and room temperature (298.15 K), the electrode configuration is hemisphere-hemisphere type with various gap widths from 1 to $25 \mu\text{m}$, and

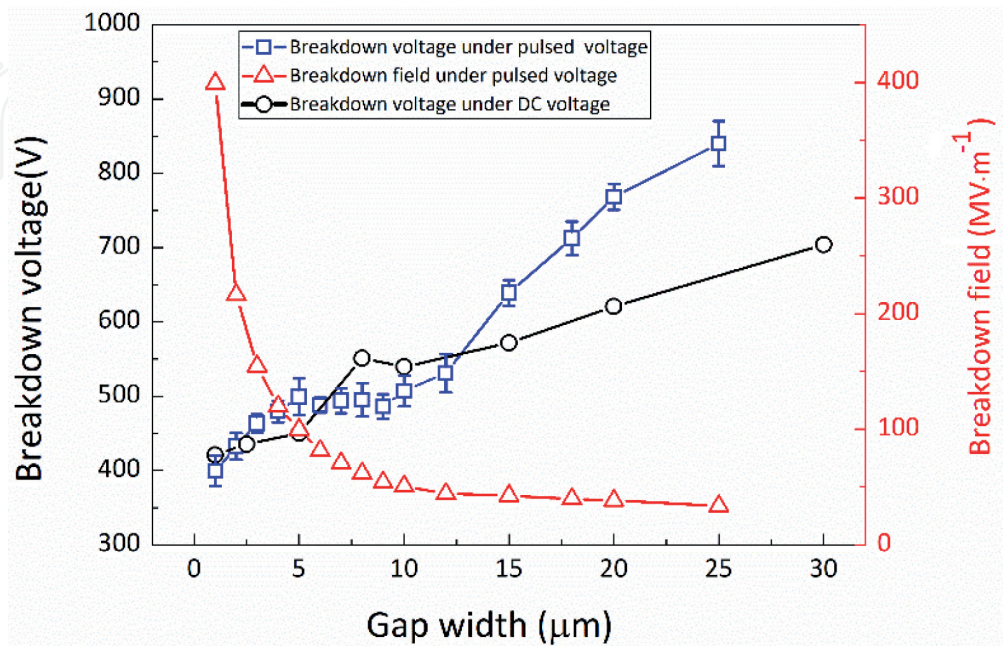


Figure 8. Breakdown thresholds as a function of gap widths under nanosecond pulsed voltage and DC voltage.

the error bars in all these figures show the standard deviation above and below the mean value of measurement. The results of pulsed breakdown [51] and DC breakdown [32] are plotted for comparisons. Generally, the nanosecond pulsed breakdown thresholds are at least two or three times higher than DC breakdown [52]; however, an interesting phenomenon can be observed from **Figure 8** when the gap width is scaled down to 15 μm . It can be seen that, overall, Actually, a lot of numerical under nanosecond pulsed voltage (blue solid square) shows a similar trend and amplitude to those under DC voltage (black solid square). For a 15- μm gap, the pulsed breakdown voltage is 639 V while the DC breakdown voltage is 571 V. For a 5- μm gap, the pulsed breakdown voltage is 450 V while the DC breakdown voltage is 499 V. More specifically, it can be noted that there is also a “plateau” stage between 5 and 10 μm , with a constant breakdown voltage of about 490 V, which is considered to be the transition region from Townsend avalanche to ion-enhanced field emission.

When the gap width is <5 μm , the breakdown voltage decreases with the decrease of gap width, demonstrating a good consistence with the DC breakdown voltage ($U_{\text{pulsed}} = 432 \text{ V} \approx U_{\text{DC}} = 435 \text{ V}$ for the 3- μm gap). Meanwhile, the pulsed breakdown voltage is found to have a power law dependence on the gap width through conducting the fitting analysis: $U = 396 \times b^{0.14}$, where U is the breakdown voltage in Volt, b is the gap width in micrometer and the Adj. R-Square is 0.99195. That is in good agreement with the vacuum breakdown behaviors proposed by Staprans in 1966 [53, 54], implying that while the gap width is reduced to 5 μm , the pulsed breakdown in air might be similar to the vacuum breakdown. So as the gap width shrinks to several micrometers, the number of gas molecules inside the gap would be not enough for the collision ionization, and thus, higher field strength is demanded for electron avalanche. When the gap width is reduced to <5 μm , the electric field strength is calculated to be 108 V/m, which has reached the threshold of field electron emission from the electrode surface. The obvious transition in the curves can be noticed and the cathode field emission is believed to play a dominant role in the generation of free electrons.

However, as the gap width continues to increase from 15 μm , it is noteworthy that pulsed breakdown demonstrates larger thresholds, and furthermore exhibits a linear increase with a positive slope of 21.5 compared to the positive slope of 8.4 for the DC breakdown voltages, which indicates that the duration of applied voltage determines the amplitude of breakdown voltage [55], that is, the breakdown under the nanosecond pulse would be much more difficult to breakdown than the DC voltage, and thus, it could be expected to become two or three times larger than the DC breakdown values as mentioned above.

3.3 The effect of atmospheric pressures

Figure 9 shows the breakdown thresholds as a function of atmospheric pressures [56], the squares represent the breakdown thresholds at a pressure of 760 Torr, the circles represent the breakdown thresholds at a pressure of 375 Torr, and the triangles represent the breakdown thresholds at a pressure of 23 Torr. The electrode configuration is hemisphere-hemisphere type with various gap widths from 1 to 25 μm . Apparently, the curves demonstrate a similar trend; however, the breakdown voltages are almost the same when the gap width is <5 μm . Considering an electron as the gas molecule, the mean free path of an electron λ_e can be derived from the following equation.

$$\lambda_e = \frac{K_B \cdot T}{\pi \left(\frac{d_m + d_e}{2} \right)^2 \cdot p} \quad (2)$$

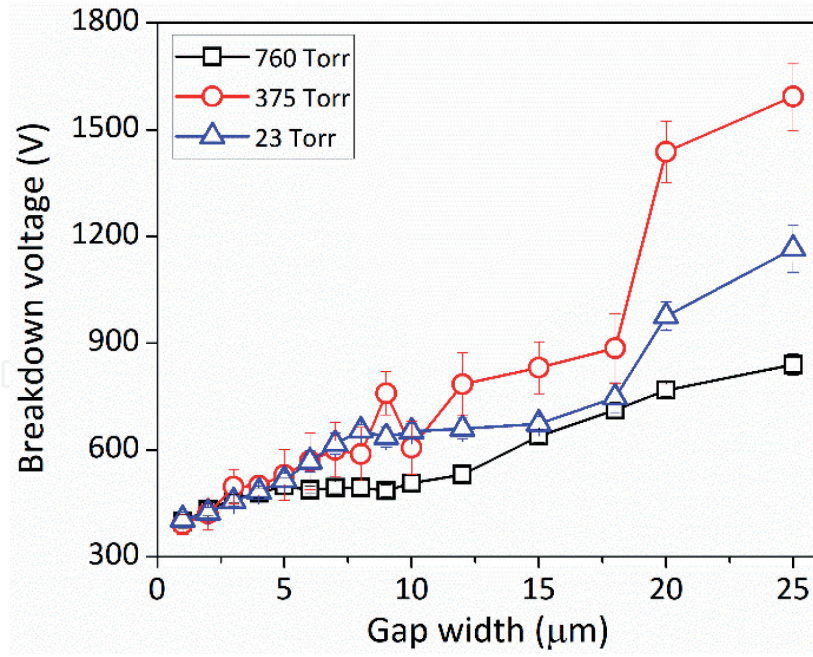


Figure 9.
Breakdown voltages as a function of gas pressure at different pressures.

where K_B is the Boltzmann constant (1.38×10^{-23} J/K), T is the ambient temperature in Kelvins, d_m is the atom or molecular diameter in meter, d_e is the electron diameter in meter, and p is the atmospheric pressure in Pascal. Since d_e is 5.62×10^{-15} m which is $<1/1000$ of the proton diameter, the collision between electrons could be neglected, so the mean free path of an electron could be defined to be the average distance the electron travels between successive collisions with the gas atom or molecule, that is, $\lambda_e = \frac{K_B \cdot T}{\pi \left(\frac{d_m}{2}\right)^2 \cdot p}$, which is inversely proportional to the square of the gas molecule diameter [57]. According to Eq. (2), when the gas pressure is 760, 375, and 23 Torr, the mean free path of an electron in air is calculated to be 539 nm, 1.1 μ m, and 18 μ m, respectively, which are either much smaller or comparable with the gap length (5 μ m), so the moving electrons can seldom collide with the gas molecules in the gap space and the number of collisions is so small that no considerable electrons and ions could be produced, in other words, the gaseous gap is almost equivalent to vacuum gap at this scale. As the gap width increases, sufficient and more collision ionization can take place at 760 Torr than those at 23 and 375 Torr due to larger propagation distances (>5 μ m), which result in the significant difference between the breakdown thresholds. This implies that the role of gas molecule density or atmospheric pressure inside the gap could be eliminated when the gap width is <5 μ m but will greatly affect the breakdown process in larger gaps. However, it also demonstrates a different trend that the breakdown thresholds at 375 Torr are larger than those at 23 Torr, which will be further investigated in the future study.

4. The dynamics of electrical breakdown in microgaps

Except for the fundamental properties of electrical breakdown in microgaps, the breakdown evolution process was also investigated for further understanding the dynamics properties, with the aid of the in-situ electro-optical measurement system introduced in Section 2.5. This section provides the temporal evolution of gas breakdown which exhibits various breakdown channel morphologies and transitions dependent upon the gap width, and highlights the breakdown dynamics in microgaps.

4.1 The breakdown paths

Figure 10 shows the breakdown morphology and discharge paths for various gap widths ranging from 1 to 20 μm . The sphere-sphere electrodes are employed in the atmospheric air environment, and the triggering time of the ICCD shutter is 10 μs prior to the breakdown moment with an exposure time of 200 ms, which guarantees that the entire breakdown process could be captured and recorded within one shot. It can be seen from **Figure 10a–c** with a gap width of 20, 15, and 12 μm , that the luminescence fills the entire gap and surroundings, in which an intense light channel can be clearly observed between the electrodes. Typically, the discharge plasma would propagate along the shortest distance between the electrodes, and the spot with maximum electric field strength is at the apex of the sphere electrodes, so the straight line connecting the apexes is considered to be the shortest path for the breakdown, which could be proved by the captured images. However, an interesting phenomenon is observed in **Figure 10d–f** with a gap width of 9, 7, and 5 μm , that the intense light channel does not follow the very straight line between the electrodes; on the contrary, it initiates from the cathode apex and propagates along a curved line

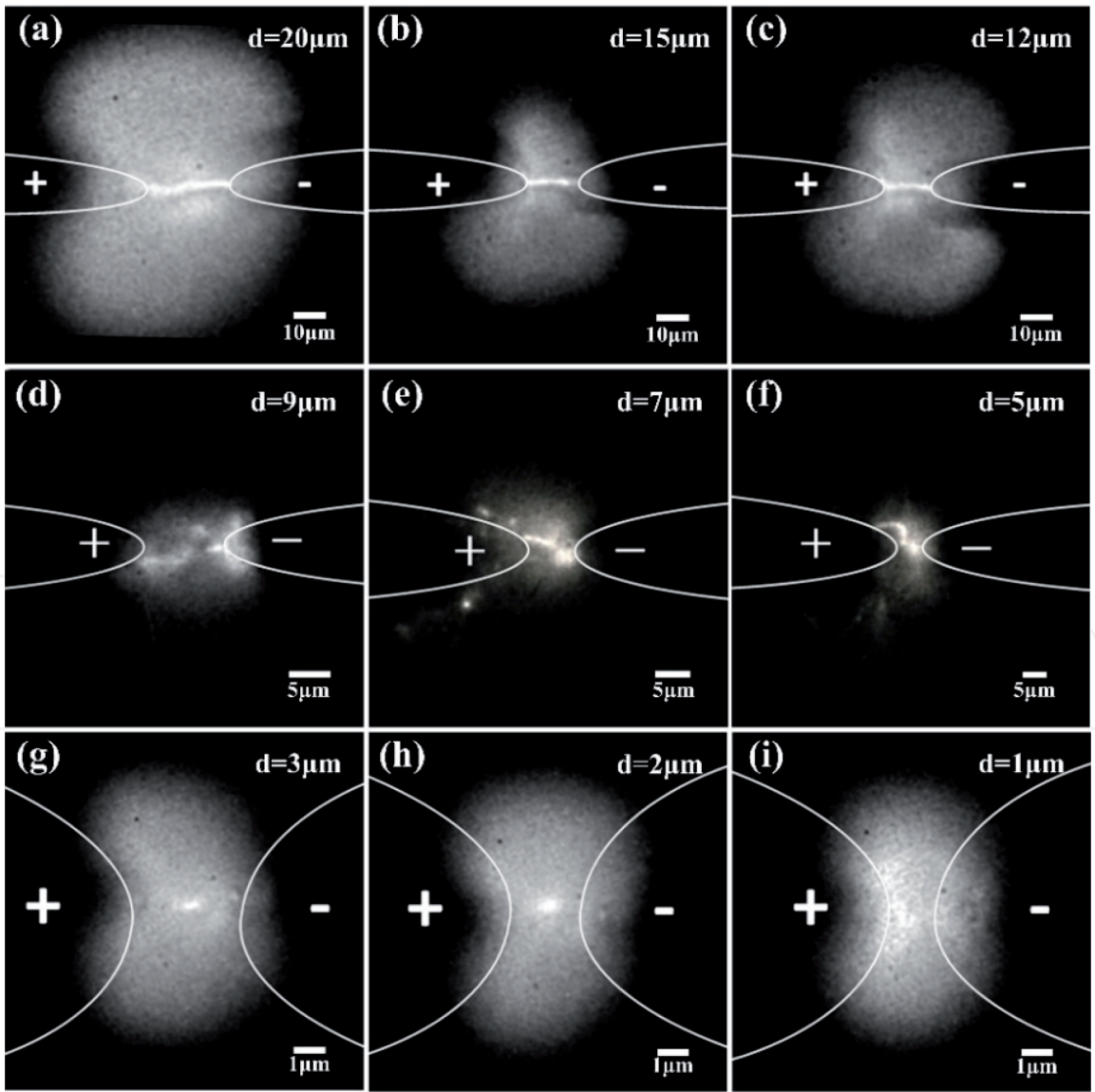


Figure 10. Breakdown morphology at gap widths from 1 to 20 μm . (a–c) show the breakdown propagating along the shortest path with luminescence filling the surrounding area, (d–f) show the roughly constant path lengths regardless of gap width which is consistent with the plateau of breakdown voltage in this region, and (g–i) indicate no obvious breakdown channel arising at these smallest gap distances [48].

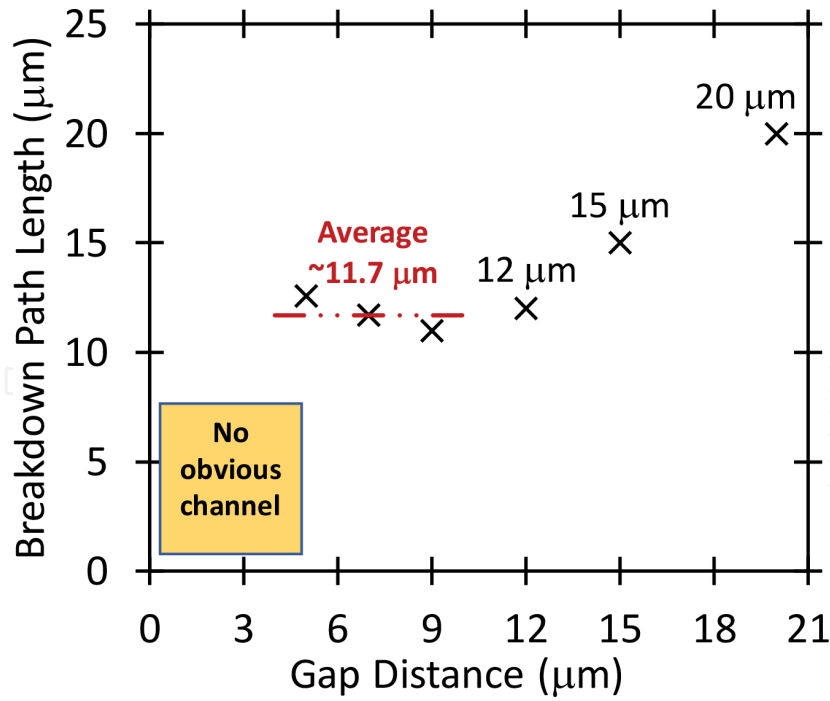


Figure 11.
The effective lengths of breakdown path for various gap widths [48].

to the neighbor region of the anode apex, which is a significant deviation from the theoretical prediction. In **Figure 10g–i** with a gap width of 3, 2, and 1 μm, the entire gap is full of luminescence and no obvious breakdown channel could be observed. While a channel may arise for the 2 and 3 μm gaps, it is much fainter compared to overall luminous intensity of the remainder of the diffuse discharge, unlike the noticeably higher intensity channels that connect both electrodes at larger gaps [48].

Figure 11 shows the effective lengths of breakdown paths in different gaps according to the breakdown channel images in **Figure 10**. It can be noteworthy that the curved path in **Figure 10d–f** is almost the same (about 11.7 μm) regardless of the gap widths, which is well consistent with the trend of the breakdown voltages in **Figure 7** and would be a very straight evidence to explain the “plateau” stage from 5 to 10 μm. That is, the consistency between the plateau in breakdown voltage and the constant breakdown path length for gap widths ranging from 5 to 10 μm is critical for understanding the transition in breakdown mechanism both experimentally and theoretically. It implies that the extension of breakdown path provides more collision ionization and electron avalanches for the breakdown which means that the ion-enhanced field emission must play an important role in breakdown rather than the Townsend avalanche alone, thus resulting in the “plateau” stage. Therefore, this evidence directly shows the transition from Townsend avalanche to ion-enhanced field emission, in which the field emission begins to dominate over Townsend avalanche for gaps smaller than ~10 μm and Townsend avalanche becomes continuously less important for smaller gaps, and finally, the field emission will dominate the breakdown for gaps shorter than 5 μm [48].

5. The physical mechanism of electrical breakdown in microgaps

Based on the captured breakdown morphology across various microgaps, the physical mechanisms could be summarized as follows:

- a. When the gap width d is larger than 10 μm, the breakdown threshold is expressed as a function of the product gas pressure p and gap width d , and the

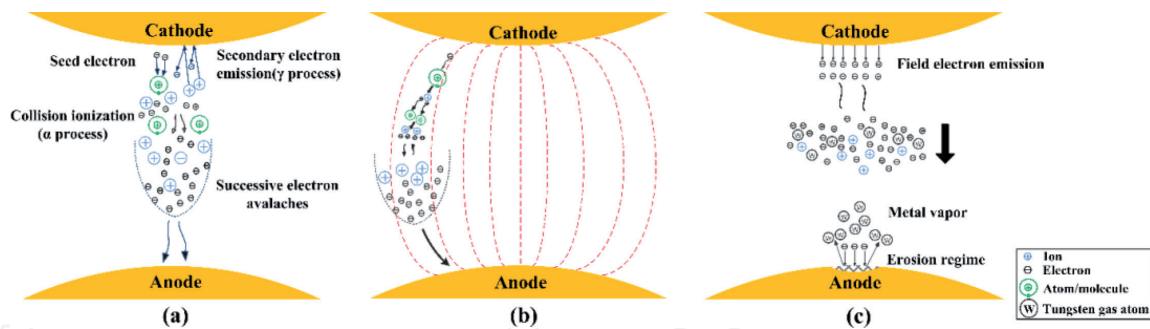


Figure 12. The physical process unifying Townsend avalanche and field emission for microscale breakdown for (a) $d > 10 \mu\text{m}$, (b) $d = 5\text{--}10 \mu\text{m}$, and (c) $d = 1\text{--}5 \mu\text{m}$ [48].

Townsend avalanche is considered to be the dominant mechanism. The breakdown demonstrates a clear electron avalanche plasma trajectory connecting the cathode tip and the anode tip by a straight path, as shown in **Figure 12a**.

- b. When the gap width d lies between 10 and $5 \mu\text{m}$, Townsend avalanche still plays a role in breakdown but the contribution of ion enhanced field emission becomes more important. In this regime, a plateau can be observed indicating that the breakdown thresholds almost remain invariant as the decrease of the gap width, which shows the transient from Townsend avalanche to the field emission process. Although the gap length is not long enough for the collision ionization, the initial electron avalanche is generated in the vicinity of the cathode and propagates along a curved path following the electric field lines. This could extend the effective propagation width and then may increase the collision ionization probability and frequency. The successive electron avalanches would be produced and may ultimately contribute to inducing breakdown, as shown in **Figure 12b**.
- c. When the gap width d is smaller than $5 \mu\text{m}$, the breakdown threshold demonstrates a linear relationship with the gap width. In this regime, a high electric field ($\sim 10^8 \text{ V/m}$) would reduce the potential barrier of the cathode and electrons would be emitted into the gap, so the initial electron avalanche can be generated around the cathode tip. Since the electron mean free path is comparable to the gap length, the emitted electrons would drift toward the anode and collide with the anode directly, resulting in the heating and release of anode and cathode materials due to the Nottingham effect. Then the thermal electron emission would turn on and more electrons would be generated by the combination of field emission and thermal emission. The outgas and atoms would fill the gap, and finally breakdown would occur with a steep decline of predicted voltage thresholds, which indicates that field emission is the dominated mechanism for gap width $< 5 \mu\text{m}$, as shown in **Figure 12c**.

6. Summary and outlook

This chapter provides a general review of the electrical breakdown in microgaps, including the methodology, influencing factors, dynamics, and physical mechanism. The breakdown thresholds in various conditions and the transition from Townsend avalanche to field emission-driven breakdown were demonstrated, which would be vital to the electrical breakdown theory at microscale. Meanwhile, understanding the fundamental mechanism of gas breakdown at microscale will have far reaching impact on practical devices due to the numerous applications that

leverage microplasmas [21], including excimer lamps with emissions in the VUV [58], ozone generators [59], arrays for flat panel light sources [60], nanoparticle synthesis [61], medicine [62], environmental remediation [63], detectors [64, 65], microthrusters [66], and combustion [67]. While a lot of numerical calculation work devoted to this subject could be found in somewhere else, this chapter focuses on the experimental investigations of breakdown behaviors in microgaps, which helps to pave the way for insulation design and discharge applications at small scales.

As the miniaturization trend of devices and equipment continues along with the great demand in civil and military industries, the electrostatic sensitivity increases accordingly, leading to a new failure mechanism [26]. When the physical size downscales to nanoscale and molecular scale, the quantum effect, space charge effect, and other effects should be considered, and this will also require novel experimental techniques that can obtain more physical parameters during the breakdown process. Therefore, with advanced experimental techniques, more and more explorations in breakdown behaviors at microscale, nanoscale, and molecular scale will surely be carried out, and new physical mechanisms will be put forward in the future.

Acknowledgements

This chapter was supported by the National Natural Science Foundation of China (Grant No. 51607138, 51521065), the Fundamental Research Funds for the Central Universities (Grant No. xzy012019030), and China Postdoctoral Science Foundation (Grant No. 2016M602820).

Conflict of interest


The authors declare that there is no conflict of interest regarding the publication of this chapter.

Author details

Guodong Meng* and Yonghong Cheng
Xi'an Jiaotong University, Xi'an, China

*Address all correspondence to: gdmengxjtu@xjtu.edu.cn

IntechOpen

© 2019 The Author(s). Licensee IntechOpen. This chapter is distributed under the terms of the Creative Commons Attribution License (<http://creativecommons.org/licenses/by/3.0>), which permits unrestricted use, distribution, and reproduction in any medium, provided the original work is properly cited. 

References

- [1] Brock DC, Moore GE. Understanding Moore's Law: Four Decades of Innovation. San Francisco: Chemical Heritage Foundation; 2006. DOI: 10.5860/choice.44-6278
- [2] Rebeiz GM, Muldavin JB. RF MEMS switches and switch circuits. *IEEE Microwave Magazine*. 2001;2(4):59-71. DOI: 10.1109/6668.969936
- [3] Bilici MA, Haase JR, Boyle CR, Go DB, Sankaran RM. The smooth transition from field emission to a self-sustained plasma in microscale electrode gaps at atmospheric pressure. *Journal of Applied Physics*. 2016;119(22):223301. DOI: 10.1063/1.4953648
- [4] Steinman A. Reducing electrostatic related defects in photolithography. In: *IEEE International Symposium on Semiconductor Manufacturing*; 1994. DOI: 10.1109/ISSM.1994.729449
- [5] Montoya J, Levit L, Englisch A. A study of the mechanisms for ESD damage to reticles. *IEEE Transactions on Electronics Packaging Manufacturing*. 2001;24(2):78-85. DOI: 10.1109/6104.930957
- [6] Wallash A. A study of shunt ESD protection for GMR recording heads. *Journal of Electrostatics*. 2002;56(3):295-302. DOI: 10.1016/S0304-3886(02)00091-8
- [7] Wallash A, Levit L. Electrical breakdown and ESD phenomena for devices with nanometer-to-micron gaps. In: *Reliability, Testing, and Characterization of MEMS/MOEMS II*; 2003. pp. 87-96. DOI: 10.1117/12.478191
- [8] Wallash A et al. Electrostatic discharge testing of tunneling magnetoresistive (TMR) devices. *IEEE Transactions on Magnetics*. 2000;36(5):2809-2811. DOI: 10.1109/20.908596
- [9] Voldman SH. ESD Basics: From Semiconductor Manufacturing to Product Use. Chichester: John Wiley & Sons; 2012. DOI:10.1002/9781118443323
- [10] Tazzoli A et al. A comprehensive study of MEMS behavior under EOS/ESD events: Breakdown characterization, dielectric charging, and realistic cures. In: *IEEE Electrical Overstress/Electrostatic Discharge Symposium Proceedings*; 2010. DOI: 10.1016/j.elstat.2011.07.007
- [11] Sangameswaran S et al. A study of breakdown mechanisms in electrostatic actuators using mechanical response under EOS-ESD stress. In: *IEEE 31st EOS/ESD Symposium*; 2009
- [12] Tazzoli A, et al. EOS/ESD sensitivity of functional RF-MEMS switches. In: *IEEE 30th Electrical Overstress/Electrostatic Discharge Symposium*; 2008
- [13] Tazzoli A, Peretti V, Meneghesso G. Electrostatic discharge and cycling effects on ohmic and capacitive RF-MEMS switches. *IEEE Transactions on Device and Materials Reliability*. 2007;7(3):429-437. DOI: 10.1109/tdmr.2007.907422
- [14] Walraven JA, et al. Electrostatic discharge/electrical overstress susceptibility in MEMS: A new failure mode. In: *Proceedings SPIE 4180, MEMS Reliability for Critical Applications*; 2000. pp. 30-39. DOI: 10.1117/12.395703
- [15] Walraven JA, et al. Human body model, machine model, and charge device model ESD testing of surface micro machined microelectromechanical systems (MEMS). In: *IEEE Electrical Overstress/Electrostatic Discharge Symposium*; 2001
- [16] Sangameswaran S, et al. ESD reliability issues in

- microelectromechanical systems (MEMS): A case study on micromirrors. In: IEEE 30th Electrical Overstress/Electrostatic Discharge Symposium; 2008
- [17] Sangameswaran S et al. Impact of design factors and environment on the ESD sensitivity of MEMS micromirrors. *Microelectronics Reliability*. 2010;**50** (9-11):1383-1387. DOI: 10.1016/j.microrel.2010.07.079
- [18] Cheng Y, Meng G, You XG, Chen L, Wu K, Pan C. Experimental study on electrical breakdown of micro-electromechanical systems with micro-gaps. In: 2012 Annual Report Conference on Electrical Insulation and Dielectric Phenomena; 2012. pp. 339-342. DOI: 10.1109/CEIDP.2012.6378790
- [19] Steinman A, Henry LG, Hernandez M. Measurements to establish process ESD compatibility. In: IEEE Electrical Overstress/Electrostatic Discharge Symposium; 2010
- [20] Schoenbach KH, Becker K. 20 years of microplasma research: A status report. *The European Physical Journal D*. 2016;**70**(2):29. DOI: 10.1140/epjd/e2015-60618-1
- [21] Becker K. Microplasmas, a platform technology for a plethora of plasma applications. *The European Physical Journal Special Topics*. 2017;**226**(13):2853-2858. DOI: 10.1140/epjst/e2016-60375-4
- [22] Charles C, Bish A, Boswell R, Dedrick J, Greig A, Hawkins R, et al. A short review of experimental and computational diagnostics for radiofrequency plasma micro-thrusters. *Plasma Chemistry and Plasma Processing*. 2016;**36**(1):29-44. DOI: 10.1007/s11090-015-9654-5
- [23] Wright W, Ferrer P. Electric micropropulsion systems. *Progress in Aerospace Sciences*. 2015;**74**:48-61. DOI: 10.1016/j.paerosci.2014.10.003
- [24] Levchenko I, Xu S, Teel G, Mariotti D, Walker M, Keidar M. Recent progress and perspectives of space electric propulsion systems based on smart nanomaterials. *Nature Communications*. 2018;**9**(1):879. DOI: 10.1038/s41467-017-02269-7
- [25] Martinez-Sanchez M, Pollard JE. Spacecraft electric propulsion-an overview. *Journal of Propulsion and Power*. 1998;**14**(5):688-699. DOI: 10.2514/2.5331
- [26] Voldman SH. Nano electrostatic discharge. *IEEE Nanotechnology Magazine*. 2009;**3**(3):12-15. DOI: 10.1109/MNANO.2009.934212
- [27] Voldman SH. *Electrical Overstress (EOS): Devices, Circuits and Systems*. Chichester: John Wiley & Sons; 2013. DOI: 10.1002/9781118511886
- [28] Voldman SH. *ESD: Failure Mechanisms and Models*. Chichester: John Wiley & Sons; 2009. DOI:10.1002/9780470747254
- [29] Paschen F. On sparking over in air, hydrogen, carbon dioxide under the potentials corresponding to various pressures. *Wiedemann Annalen der Physik und Chemie*. 1889;**37**:69-96
- [30] Boyle W, Kisliuk P. Departure from Paschen's law of breakdown in gases. *Physical Review*. 1955;**97**(2):255-259. DOI: 10.1103/PhysRev.97.255
- [31] Iwabuchi H, Morimoto T, Matsuoka S, Kumada A, Hidaka K. Pre-breakdown phenomenon in micrometer-scale gap. In: 31st ICPIG; 2013
- [32] Radmilović-Radjenović M, Matejčik Š, Klas M, Radjenović B. The role of the field emission effect in direct-current argon discharges for the gaps ranging from 1 to 100 μm . *Journal of Physics D: Applied Physics*. 2012;**46**(1):015302. DOI: 10.1088/0022-3727/46/1/015302

- [33] Li Y, Tirumala R, Rumbach P, Go DB. The coupling of ion-enhanced field emission and the discharge during microscale breakdown at moderately high pressures. *IEEE Transactions on Plasma Science*. 2013;**41**(1):24-35. DOI: 10.1109/TPS.2012.2224380
- [34] Venkatraman A, Garg A, Peroulis D, Alexeenko AA. Direct measurements and numerical simulations of gas charging in microelectromechanical system capacitive switches. *Applied Physics Letters*. 2012;**100**(8):083503. DOI: 10.1063/1.3688176
- [35] Venkatraman A, Alexeenko AA. Scaling law for direct current field emission-driven microscale gas breakdown. *Physics of Plasmas*. 2012;**19**(12):123515. DOI: 10.1063/1.4773399
- [36] Marić R, Stanković K, Vujisić M, Osmokrović P. Electrical breakdown mechanisms in vacuum diodes. *Vacuum*. 2010;**84**(11):1291-1295. DOI: 10.12693/APhysPolA.118.585
- [37] Sudarshan T, Ma X, Muzykov P. High field insulation relevant to vacuum microelectronic devices. *IEEE Transactions on Dielectrics and Electrical Insulation*. 2002;**9**(2):216-225. DOI: 10.1109/94.993738
- [38] Go DB, Pohlman DA. A mathematical model of the modified Paschen's curve for breakdown in microscale gaps. *Journal of Applied Physics*. 2010;**107**(10):103303. DOI: 10.1063/1.3380855
- [39] Klas M, Matejcik S, Radjenovic B, Radmilovic-Radjenovic M. Experimental and theoretical studies of the direct-current breakdown voltage in argon at micrometer separations. *Physica Scripta*. 2011;**83**(4):045503. DOI: 10.1088/0031-8949/83/04/045503
- [40] Klas M, Matejcik S, Radjenovic B, Radmilovic-Radjenovic M. Experimental and theoretical studies of the breakdown voltage characteristics at micrometre separations in air. *Europhysics Letters*. 2011;**95**(3):35002. DOI: 10.1209/0295-5075/95/35002
- [41] Buendia JA, Venkatraman A. Field enhancement factor dependence on electric field and implications on microscale gas breakdown: Theory and experimental interpretation. *EPL (Europhysics Letters)*. 2015;**112**(5):55002. DOI: 10.1209/0295-5075/112/55002
- [42] Loveless AM, Garner AL. A universal theory for gas breakdown from microscale to the classical Paschen law. *Physics of Plasmas*. 2017;**24**(11):113522. DOI: 10.1063/1.5004654
- [43] Cheng Y, Meng G, Dong C. Review on the breakdown characteristics and discharge behaviors at the micro&nano scale. *Transactions of China Electrotechnical Society*. 2017;**32**(2):13-23. DOI: CNKI:SUN:DGJS.0.2017-02-002
- [44] Torres JM, Dhariwal RS. Electric field breakdown at micrometer separations in air and vacuum. *Microsystem Technologies*. 1999;**6**(1): 6-10. DOI: 10.1007/s005420050166
- [45] Meng G, Cheng Y, Gao X, Wang K, Dong C, Zhu B. In-situ optical observation of dynamic breakdown process across microgaps at atmospheric pressure. *IEEE Transactions on Dielectrics and Electrical Insulation*. 2018;**25**(4):1502-1507. DOI: 10.1109/TDEI.2018.007017
- [46] Strong F, Skinner JL, Tien NC. Electrical discharge across micrometerscale gaps for planar MEMS structures in air at atmospheric pressure. *Journal of Micromechanics and Microengineering*. 2008;**18**(7):075025. DOI: 10.1088/0960-1317/18/7/075025

- [47] Meng G, Cheng Y, Wu K, Chen L. Electrical characteristics of nanometer gaps in vacuum under direct voltage. *IEEE Transactions on Dielectrics and Electrical Insulation*. 2014;**21**(4): 1950-1956. DOI: 10.1109/TDEI.2014.004376
- [48] Meng G, Gao X, Loveless AM, Dong C, Zhang D, Wang K, et al. Demonstration of field emission driven microscale gas breakdown for pulsed voltages using in-situ optical imaging. *Physics of Plasmas*. 2018;**25**(8):082116. DOI: 10.1063/1.5046335
- [49] Meng G, Ying Q, Loveless AM, Wu F, Wang K, Fu Y, et al. Spatio-temporal dynamics of pulsed gas breakdown in microgaps. *Physics of Plasmas*. 2019;**26**(1):014506. DOI: 10.1063/1.5081009
- [50] Go D, Venkatraman A. Microscale gas breakdown: Ion-enhanced field emission and the modified Paschen's curve. *Journal of Physics D: Applied Physics*. 2014;**47**(50):503001. DOI: 10.1088/0022-3727/47/50/503001
- [51] Meng G. Experimental and numerical investigation of the influencing factors on pulsed gas breakdown in microgaps. In: *Preparation*; 2019
- [52] Schnyder R, Howling A, Bommottet D, Hollenstein C. Direct current breakdown in gases for complex geometries from high vacuum to atmospheric pressure. *Journal of Physics D: Applied Physics*. 2013;**46**(28):285205. DOI: 10.1088/0022-3727/46/28/285205
- [53] Lyon D, Hubler A. Gap size dependence of the dielectric strength in nano vacuum gaps. *IEEE Transactions on Dielectrics and Electrical Insulation*. 2013;**20**:1467-1471. DOI: 10.1109/TDEI.2013.6571470
- [54] Staprans A. Voltage breakdown limitations of electron guns for high power microwave tubes. In: *Proceedings of the Second International Symposium Insulation of High Voltages Vacuum*; 1966. pp. 293-303
- [55] Tao S, Guangsheng S, Ping Y, Jue W, Weiqun Y, Yaohong S, et al. An experimental investigation of repetitive nanosecond-pulse breakdown in air. *Journal of Physics D: Applied Physics*. 2006;**39**(10):2192. DOI: 10.1088/0022-3727/39/10/030
- [56] Loveless AM, Meng G, Ying Q, Wu F, Wang K, Cheng Y, et al. The transition to Paschen's law for microscale gas breakdown at subatmospheric pressure. *Scientific Reports*. 2019;**9**(1):5669. DOI: 10.1038/s41598-019-42111-2
- [57] Compton KT. The mean free path of an electron in a gas and its minimum ionizing potential. *Physical Review*. 1916;**8**(4):386. DOI: 10.1103/PhysRev.8.386
- [58] Kogelschatz U. Ultraviolet excimer radiation from nonequilibrium gas discharges and its application in photophysics, photochemistry and photobiology. *Journal of Optical Technology*. 2012;**79**(8):484-493. DOI: 10.1364/JOT.79.000484
- [59] Kim K, Park S, Eden J. Self-patterned aluminium interconnects and ring electrodes for arrays of microcavity plasma devices encapsulated in Al₂O₃. *Journal of Physics D: Applied Physics*. 2007;**41**(1):012004. DOI: 10.1088/0022-3727/41/1/012004
- [60] Eun CK, Gianchandani YB. Microdischarge-based sensors and actuators for portable microsystems: Selected examples. *IEEE Journal of Quantum Electronics*. 2012;**48**(6): 814-826. DOI: 10.1109/JQE.2012.2189199
- [61] Lin L, Wang Q. Microplasma: A new generation of technology for functional nanomaterial synthesis. *Plasma Chemistry and Plasma Processing*.

2015;**35**(6):925-962. DOI: 10.1007/
s11090-015-9640-y

[62] Iza F, Kim GJ, Lee SM, Lee JK, Walsh JL, Zhang YT, et al. Microplasmas: Sources, particle kinetics, and biomedical applications. *Plasma Processes and Polymers*. 2008;**5**(4): 322-344. DOI: 10.1002/ppap.200700162

[63] Becker KH. The use of nonthermal plasmas in environmental applications. In: *Introduction to Complex Plasmas*. Berlin Heidelberg: Springer-Verlag; 2010. pp. 367-394. DOI: 10.1007/978-3-642-10592-0

[64] Zhu Z, Chan GC-Y, Ray SJ, Zhang X, Hieftje GM. Microplasma source based on a dielectric barrier discharge for the determination of mercury by atomic emission spectrometry. *Analytical Chemistry*. 2008;**80**(22):8622-8627. DOI: 10.1021/ac801531j

[65] Joffrion JB, Mills D, Clower W, Wilson CG. On-chip microplasmas for the detection of radioactive cesium contamination in seawater. *Micromachines*. 2017;**8**(9):259. DOI: 10.3390/mi8090259

[66] Baranov OO, Xu S, Xu L, Huang S, Lim J, Cvelbar U, et al. Miniaturized plasma sources: Can technological solutions help electric micropropulsion? *IEEE Transactions on Plasma Science*. 2018;**46**(2):230-238. DOI: 10.1109/TPS.2017.2773073

[67] Elkholy A, Shoshyn Y, Nijdam S, van Oijen J, van Veldhuizen E, Ebert U, et al. Burning velocity measurement of lean methane-air flames in a new nanosecond DBD microplasma burner platform. *Experimental Thermal and Fluid Science*. 2018;**95**:18-26. DOI: 10.1016/j.expthermflusci.2018.01.011